

(1) Cover page

Final Technical Report

Award Numbers: G11AP00027 and G11AP00028

Title: Structure, Seismicity, and Stress along the San Andreas Fault near
SAFOD: Collaborative Research with UW-Madison and Georgia Tech

Authors and Affiliations: Clifford Thurber
University of Wisconsin-Madison
1215 W. Dayton St.
Madison, WI 53706
Phone: (608) 262-6027, FAX: (608) 262-0693
thurber@geology.wisc.edu

Zhigang Peng
Georgia Institute of Technology
311 Ferst Drive
Atlanta, GA, 30332-0340
Phone: (404)8940231, Fax: (404)8945638
zpeng@gatech.edu

Term Covered by the Award: January 1, 2011 - December 31, 2011

Structure, Seismicity, and Stress along the San Andreas Fault near SAFOD:
Collaborative research with UW-Madison and Georgia Tech

(2) Abstract

The San Andreas Fault Observatory at Depth (SAFOD) has yielded significant new insights into the nature of the San Andreas fault (SAF). In particular, the recovery of ~ 40 meters of core containing two meters-thick zones of fault gouge and adjacent zones of damage and alteration provides a unique opportunity to characterize the physical and chemical properties of fault zone rocks from a depth where earthquakes occur, although these samples are interpreted to come from a creeping, not seismogenic, part of the fault (Hickman et al., 2007, 2008). We propose to improve our understanding of the context within which these fault zone samples existed *in-situ* by utilizing arrival times of fault zone head waves (FZHW's) and the associated direct-wave secondary arrivals (DWSA's) to (1) improve the seismic tomography image of the SAF at relatively fine scale, and (2) improve absolute location estimates for earthquakes in the region around SAFOD and in particular the drilling target earthquakes. These two tasks have interrelated goals. Primary among them is to characterize in detail the seismogenic structures on which the earthquakes near SAFOD occur and relate those structures to the borehole and core observations. There is a general consensus that the shallower of the two gouge zones is related to the fault strand along which the so-called "Hawaii" target earthquakes occur. Our improved absolute earthquake locations will either help support or refute this interpretation.

FZHW's have been used previously to constrain fault zone velocity contrasts along the SAF system based on the relative move-out of FZHW's versus DWSA's (Ben-Zion & Malin, 1991; Ben-Zion et al., 1992; McGuire & Ben-Zion, 2005; Lewis et al., 2007; Zhao & Peng, 2008; Zhao et al., 2010). Our project takes the next step in modeling FZHW and DWSA arrival times by incorporating them in a formal tomographic inversion for three-dimensional (3D) seismic velocity structure building on the work of Thurber et al. (2006) and Zhang et al. (2009). We take advantage of the dense surface and borehole seismic instrumentation around the study region, capitalize on the extensive FZHW analysis results of Zhao et al. (2010), and incorporate previously unavailable temporary array data to improve the delineation of the seismically active structures.

Our collaborative study improves the available information on the key *in-situ* structural properties of the SAF, particularly around the SAFOD target earthquakes. The updated absolute locations of earthquakes not only have significant implications for small-scale segmentation of the shallow SAF, but also can provide sufficient accuracy and precision for possible future drilling activities at SAFOD. The key questions we propose to address are the following:

- (1) What is the relationship between the zones of fault gouge and casing deformation found in SAFOD and the seismically active strands of the SAF, in particular those hosting the "Hawaii" and "San Francisco/Los Angeles" repeating earthquake clusters (Zoback et al., 2011)?
- (2) How does the structure of the SAF low-velocity zone, generally characterized as a very-low-velocity core and surrounding low-velocity damage zone, vary along strike and with depth?

(3) Main body of the report

Significance of the Project

Numerous pre-drilling geophysical site characterization studies around SAFOD have provided a wealth of information on the structure and seismicity of the SAF zone and its surroundings (Hickman et al., 2004, and references therein). The ~40 meters of core recovered in the last phase of SAFOD drilling in 2007 combined with the geophysical logs gives us an unprecedented view of the nature of the SAF in-situ (Hickman et al., 2007, and references therein). The occurrence of the 2004 Parkfield earthquake motivated additional studies of the structure and seismicity at larger scales around SAFOD (Harris & Arrowsmith, 2006, and references therein). Despite this wealth of studies, a number of key questions remain. Those most relevant to the proposed project include the following:

- (1) What is the relationship between the zones of fault gouge and casing deformation found in SAFOD and the seismically active strands of the SAF, in particular those hosting the "Hawaii" and "San Francisco/Los Angeles" (SF/LA) repeating earthquake clusters (Zoback et al., 2011)?
- (2) How does the structure of the SAF low-velocity zone, generally characterized as a very-low-velocity core and surrounding low-velocity damage zone, vary along strike and with depth?
- (3) Do seismic observations, especially focal mechanisms, support the weak SAF hypothesis?

By directly addressing these key questions, our collaborative study will provide the most updated information about the 3D velocity structure around SAFOD and the absolute locations and focal mechanisms of the SAFOD target earthquakes. This will not only have significant implications for small-scale segmentation of the shallow SAF, but also can provide sufficient accuracy and precision for possible future drilling activities at SAFOD. One of the USGS/EHP's long-term goals is to mitigate earthquake losses in the US by performing basic and applied research to better understand the earthquake process and the effects of earthquakes. Our proposed work would directly contribute to the USGS's long-term efforts at Parkfield on understanding earthquake phenomena and evaluating earthquake hazards through the Parkfield Earthquake Prediction Experiment and the SAFOD project.

Background

A suite of recent studies lays the foundation for the work proposed here. The local-scale tomography study of Zhang et al. (2009) for a roughly 10 km³ volume centered on SAFOD and the more regional-scale study of Thurber et al. (2006) for a 130 km x 120 km x 20 km volume centered on the 2004 Parkfield earthquake rupture provide what are probably the best 3D images of the seismic velocity structure of the area. The former shows a low velocity zone (LVZ) associated with the SAF extending to significant depth (Figure 1a), whereas the latter images the well-known velocity contrast across the fault (Figure 1b). Both studies used double-difference (DD) tomography (Zhang & Thurber, 2003) in an effort to sharpen the structure in the earthquake source regions.

These studies and the previous study by Thurber et al. (2004) also provide what are likely the most accurate and precise locations for the earthquakes around SAFOD, including the "target" earthquakes, and for the seismicity around the 2004 rupture zone (Figures 1 and 2). Subsequent unpublished work provided the final absolute locations for the target earthquakes that were used to define the Phase 3 (summer 2007) drilling trajectory. The drilling strategy was to cross the Hawaii strand ~100 m above the Hawaii hypocenters and then cross the SF/LA strand a comparable distance below those hypocenters. S-P times from $M < 0$ aftershocks of a Hawaii target event recorded by a 3-component sensor in the Phase 3 SAFOD borehole confirmed that the Hawaii cluster is indeed about 100 m below the borehole (Figure 3). Debate remains, however, about the along-strike position of the Hawaii main shock, and there is greater uncertainty about the absolute locations of the SF/LA clusters (Zoback et al., 2011).

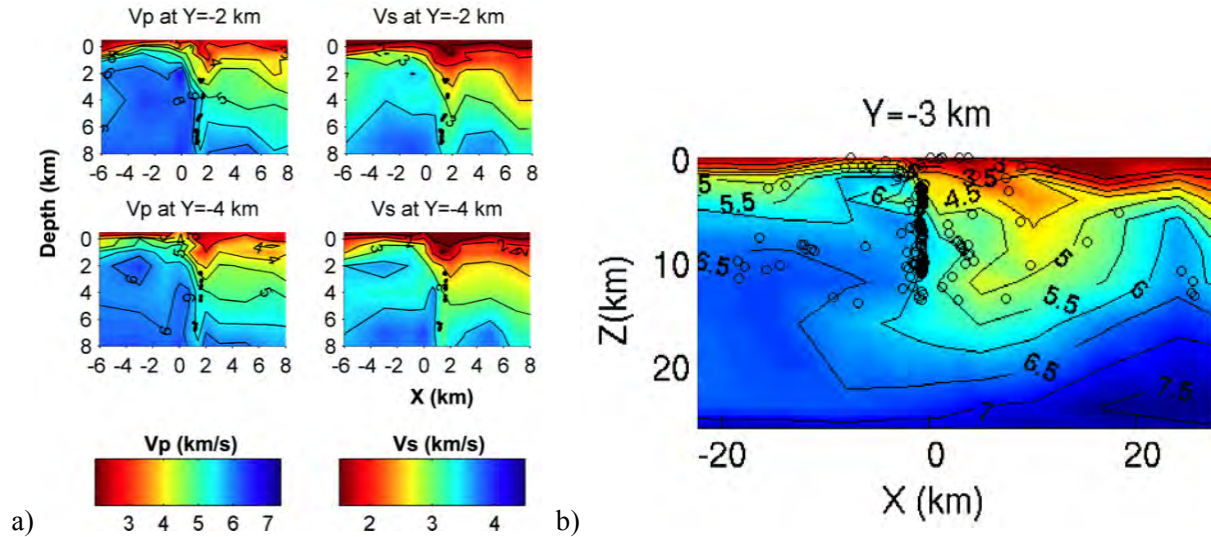


Figure 1. (a) Representative cross-sections through the local scale 3D Vp and Vs models of Zhang et al. (2009) southwest of SAFOD (which is located at X=0, Y=0 in this model) showing a deeply penetrating LVZ along the SAF. (b) Portion of a representative cross-section through the regional scale 3D Vp model of Thurber et al. (2006) near SAFOD showing the well known velocity contrast across the SAF, with the SW side faster. For this model, the coordinate origin is at Middle Mountain.

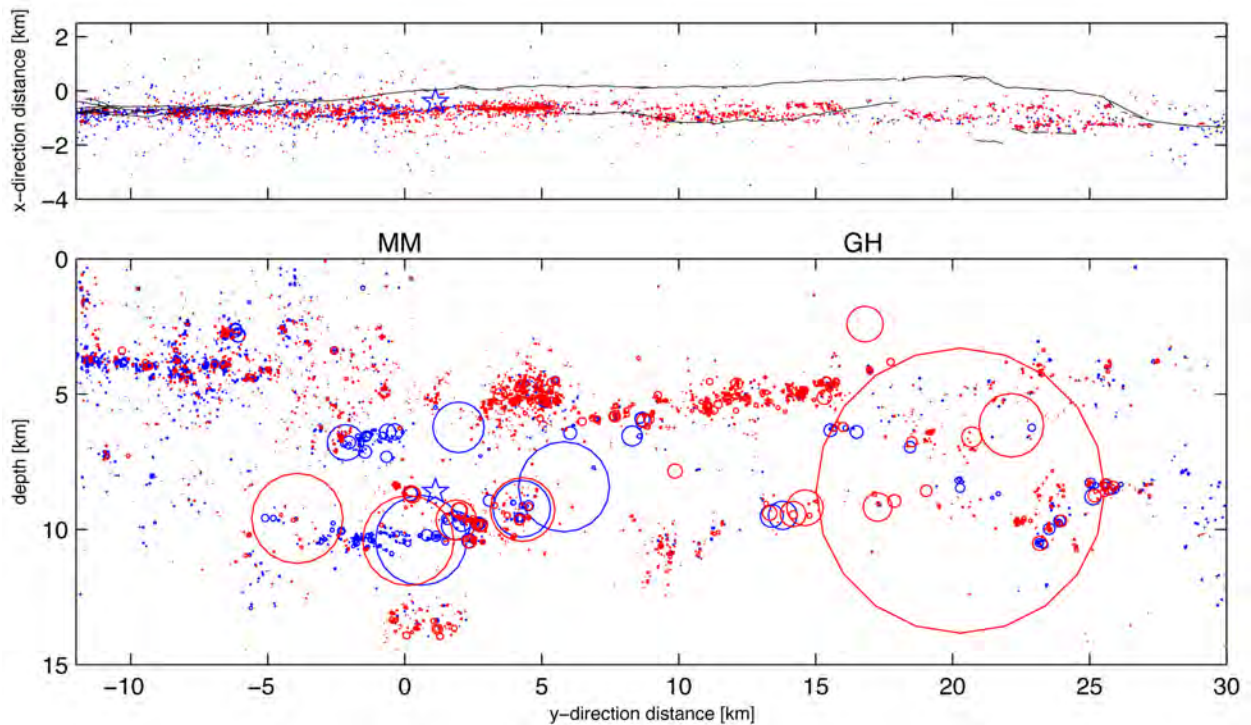


Figure 2. (top) Map view and (bottom) along-fault cross-section of DD-relocated seismicity along and northwest of the 2004 Parkfield rupture zone, covering the time period 1984-2005. The blue star is the 1966 main shock hypocenter. Blue circles are events from 1984 to the 2004 main shock, and red circles are the 2004 main shock and its aftershocks. In the cross section, circles indicate size of a model circular source with a 30 bar stress drop. From Thurber et al. (2006).

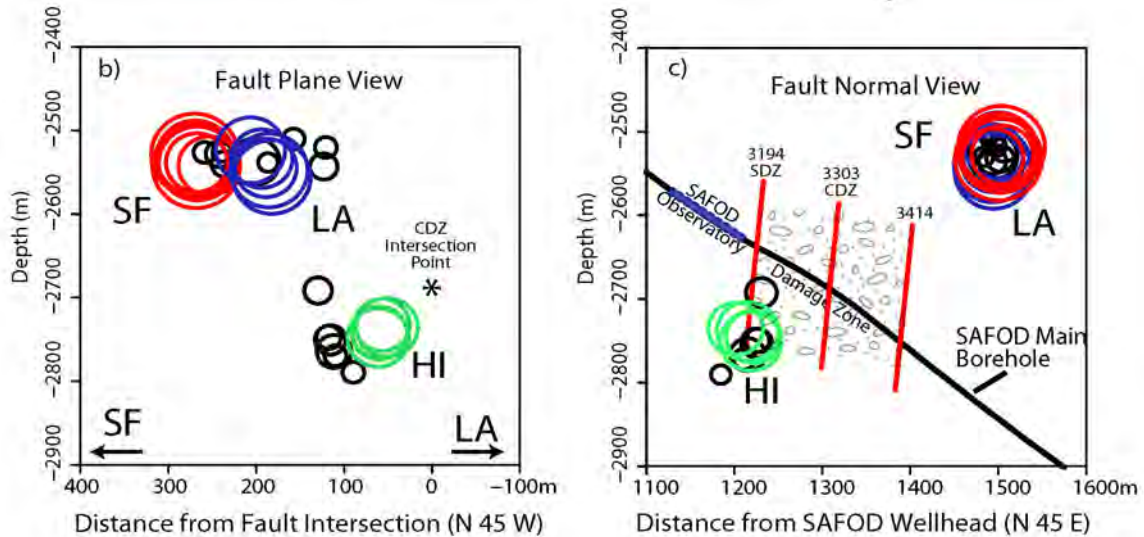


Figure 3. Fault-parallel and fault-normal cross-sections showing the positions of the Hawaii (HI) and SF/LA target earthquake clusters relative to the SAFOD main borehole. From Zoback et al. (2011).

At a larger scale, Thurber et al. (2006) studied in detail the spatial distribution of seismicity along and near the 2004 Parkfield earthquake rupture. Their study confirms the predominance of streaks and clusters in the pattern of seismicity as viewed along fault strike (Figure 2), as was previously reported by Waldhauser et al. (2004), but now including the 2004 aftershocks. The overlap between the background seismicity and the 2004 aftershocks is remarkable, and this overlap appears to extend all the way back to the 1966 aftershocks (Thurber et al., 2006). Thus these streaks and clusters are stable features that have survived for more than an entire earthquake cycle, demonstrating that these patches that fail as aftershocks (but also as background earthquakes) require no special process specifically related to the main shock (e.g., transient fluid flow or stress changes) in order to occur, although their temporal occurrence patterns do show clear correlations with the main shock (e.g. Lengliné & Marsan, 2009).

Fault zone head waves

Large crustal faults such as the SAF typically juxtapose rocks of significantly different elastic properties, resulting in well-defined bimaterial interfaces. A sharp material contrast across the fault interface is expected to generate FZHW's that spend a large portion of their propagation paths refracting along the bimaterial interface (Ben-Zion 1989, 1990; Ben-Zion & Aki 1990). The head waves propagate with the velocity and first-motion polarity of the faster block, and are radiated from the fault to the slower velocity block where they are characterized by an emergent waveform with opposite first-motion polarity to that of the direct body waves. Since FZHW spend most of their propagation paths along the fault interface, they provide a high-resolution tool for imaging the velocity contrast across the major crustal faults (Ben-Zion & Malin, 1991; Ben-Zion et al., 1992; McGuire & Ben-Zion, 2005; Lewis et al., 2007; Zhao & Peng, 2008; Zhao et al., 2010; Bulut et al., 2012).

Recently, Zhao et al. (2010) systematically analyzed large data sets of near-fault waveforms recorded by several permanent and temporary seismic networks along the Parkfield section of the SAF. They found clear FZHW's at many stations on the NE side of the SAF near SAFOD, indicating the presence of a sharp bimaterial interface in that region (Figure 4a). Based on the systematic moveout between the FZHW and DWSA, they estimated an average P-wave velocity contrast of about 5-10%. In comparison, the FZHW is not clearly developed along the SAF near Gold Hill and the average P-wave velocity contrast is estimated as 0-2% (Figure 4b). The along-strike variations of the velocity contrast (Figure 4c) are consistent with geophysical observations and geological interpretations of a sliver of high-velocity rock immediately to the NE of the SAF near GH (McLaughlin et al., 1996) and existing 3D seismic tomography results (Eberhart-Phillips & Michael, 1993; Thurber et al., 2006).

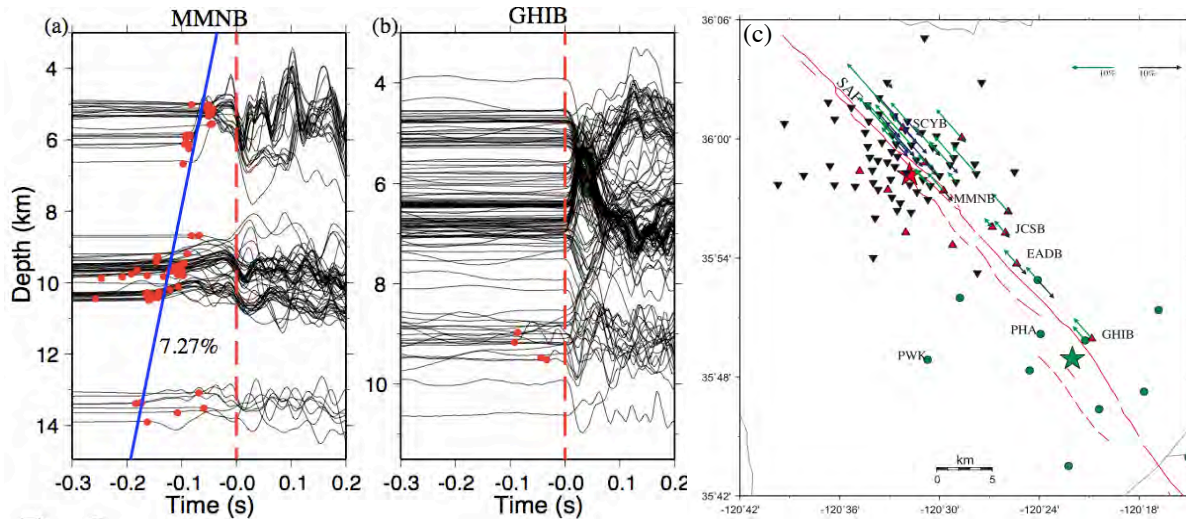


Figure 4. Vertical seismograms recorded at HRSN stations (a) MMNB and (b) GHIB showing moveout between FZHW's and DWSA's with increasing event depth, with the events approximately beneath the station. (c) A summary of the obtained velocity contrasts. The green and blue arrows represent velocity contrast values for sections to the NW and SE, respectively, centered at the corresponding stations. The length of each arrow is proportional to the velocity contrast percentage. From Zhao et al. (2010).

The local-scale tomography study of Zhang et al. (2009) for a roughly 10 km^3 volume centered on SAFOD and the more regional-scale study of Thurber et al. (2006) for a $130 \text{ km} \times 120 \text{ km} \times 20 \text{ km}$ volume centered on the 2004 Parkfield earthquake rupture provide what are probably the best 3D images of the seismic velocity structure of the area. The former shows a low velocity zone associated with the SAF extending to significant depth, and both image the well-known velocity contrast across the fault. Seismic tomography generally uses just first P and/or S arrivals because of the relative simplicity of phase picking and ray tracing. Adding secondary arrivals such as FZHW's, however, can enhance the resolution of structure and strengthen constraints on earthquake locations. In this study, we present a model of 3D velocity structure for the Parkfield region that utilizes a combination of arrival times for FZHW's and the associated direct-wave secondary arrivals as well as existing P-wave arrival time data. The resulting image provides a higher-resolution model of the SAF at depth than previously published models.

Research accomplished

We developed a preliminary model of 3D velocity structure for the Parkfield region that utilizes a combination of arrival times for FZHW's and the associated direct-wave secondary arrivals as well as existing P-wave arrival time data. Picks were made for earthquakes recorded at Parkfield between 1984 and 2005 on the Parkfield Area Seismic Observatory array, UC-Berkeley High Resolution Seismic Network, USGS Central California Seismic Network, and USGS temporary stations. Existing P-wave absolute and differential time data were from Thurber et al. (2006) and Zhang et al. (2009). The catalog of FZHW and associated direct-wave secondary arrival picks was from Zhao et al. (2010). DWSA catalog differential times were calculated from the data set of Zhao et al. (2010). The dataset is illustrated in Figure 5.

We modified the double-difference tomography algorithm *tomODD* (Zhang & Thurber, 2003) to incorporate FZHW and associated direct-wave secondary arrival times into a formal inversion for the P-wave velocity model. We have adapted the pseudo-bending method of Um & Thurber (1987) to compute travel times for both the first-arriving FZHW's and the later arriving DWSA's. The pseudo-bending method relies on the fact that for a true ray path satisfying the ray equations, the ray curvature (vector of the second spatial derivative along the path) is everywhere anti-parallel to the component of the velocity gradient normal to the ray path. The pseudo-bending strategy involves locally perturbing an approximate

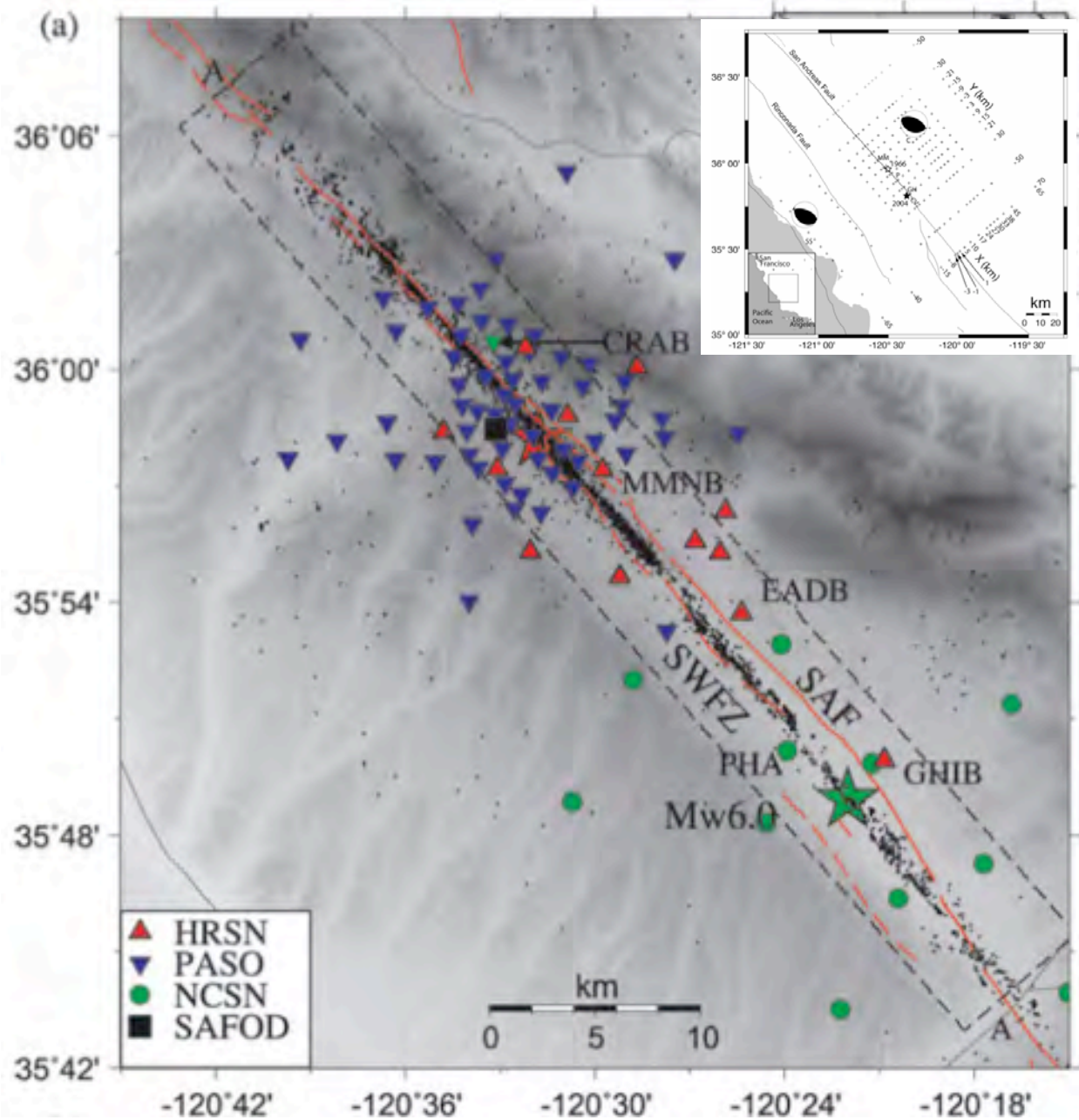


Figure 5. Dataset for our inversion, with station symbols as indicated, earthquakes as small black dots, and the location of SAFOD shown by the black square. The inset shows the X-Y coordinates.

initial ray path (determined from a brute-force search of a "web" of arcuate paths of varying dip and curvature) so that the Eikonal equation is satisfied in a piecewise manner, and iterating to convergence. The method has proven to be extremely effective when path lengths are up to ~60 km in length, with accuracies comparable to the finite-difference method (Haslinger & Kissling, 2000). The strategy for finding secondary arrivals using pseudo-bending is relatively simple. For a DWSA arrival, we can force pseudo-bending to derive the direct path instead of the FZHW path by restricting the starting path to the vertical plane connecting the earthquake and station and artificially reducing the velocities on the southwest side of the SAF. The pseudo-bending algorithm will thus converge to what is a local-minimum DWSA path instead of the global minimum FZHW path.

Selected before and after (i.e., without and with DWSA's) images of the velocity structure along fault-normal cross-section through the SAF are shown in Figure 6, along with the changes to the model. It can be clearly seen that the inclusion of the DWSA's results in an increase in the velocity contrast across the fault, as expected.

It is also of interest to quantify the across-fault contrast and compare it to other observables related to fault zone properties and behavior. Figure 7 shows the velocities just NE of the SAF, the velocities just SW of the SAF, and the across-fault contrast. Note that the area between the 1966 and 2004 Parkfield hypocenters is an area of negative contrast (NE side fast), corresponding to a high-velocity body on the NE side of the fault, as has been reported previously (Eberhart-Phillips & Michael, 1993; Thurber et al., 2006). In Figure 8, this velocity contrast is compared to the distribution of microseismicity, b-value, and the 2004 rupture.

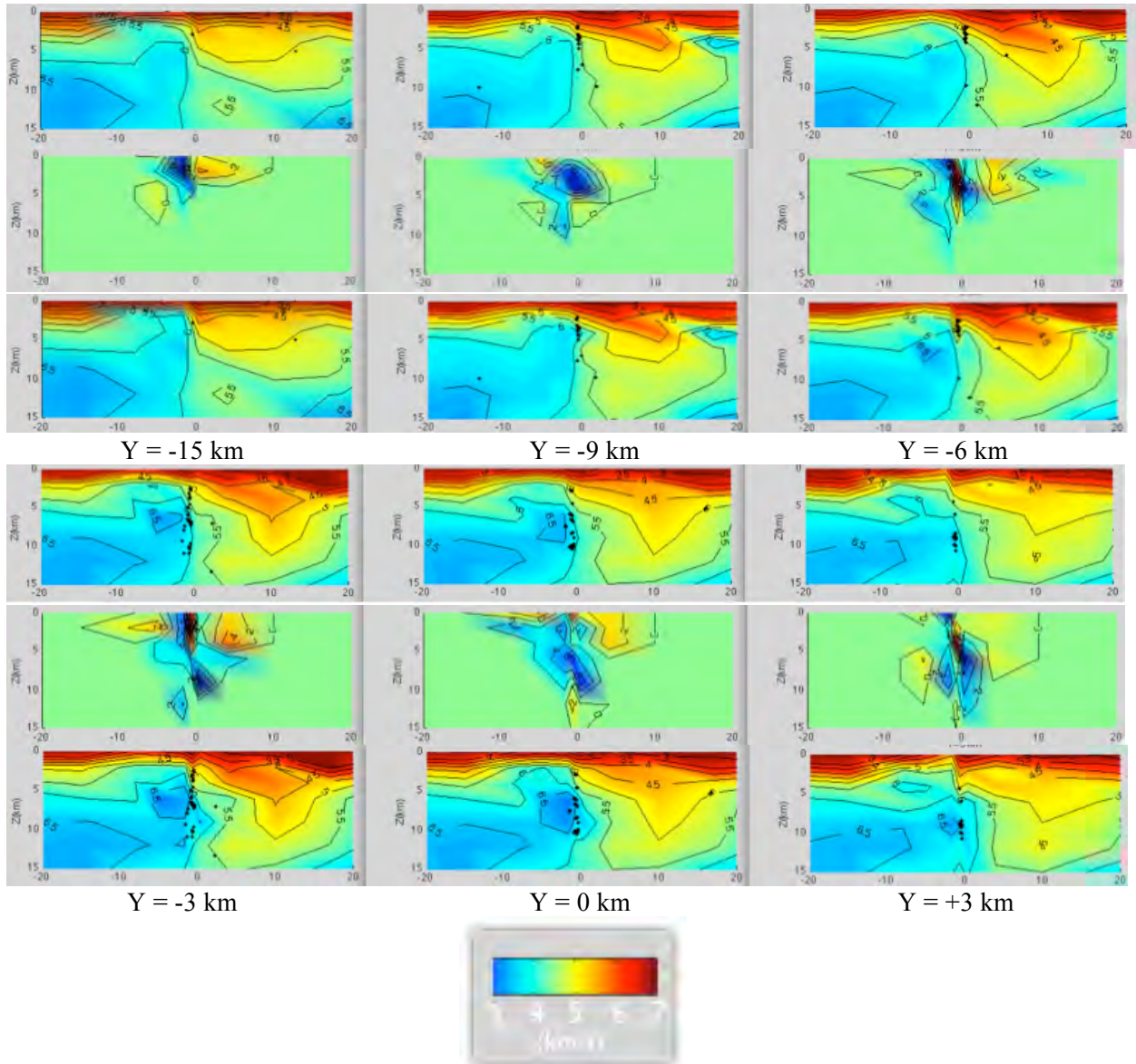


Figure 6. SW-NE cross-sections through the SAF at the indicated Y coordinate values (see inset in Figure 5) showing in each panel (top) the original model, (middle) the model perturbation from adding DWSA's, and (bottom) the new model including the DWSA's. Note the increased velocity contrasts along the fault resulting from the inclusion of the DWSA's.

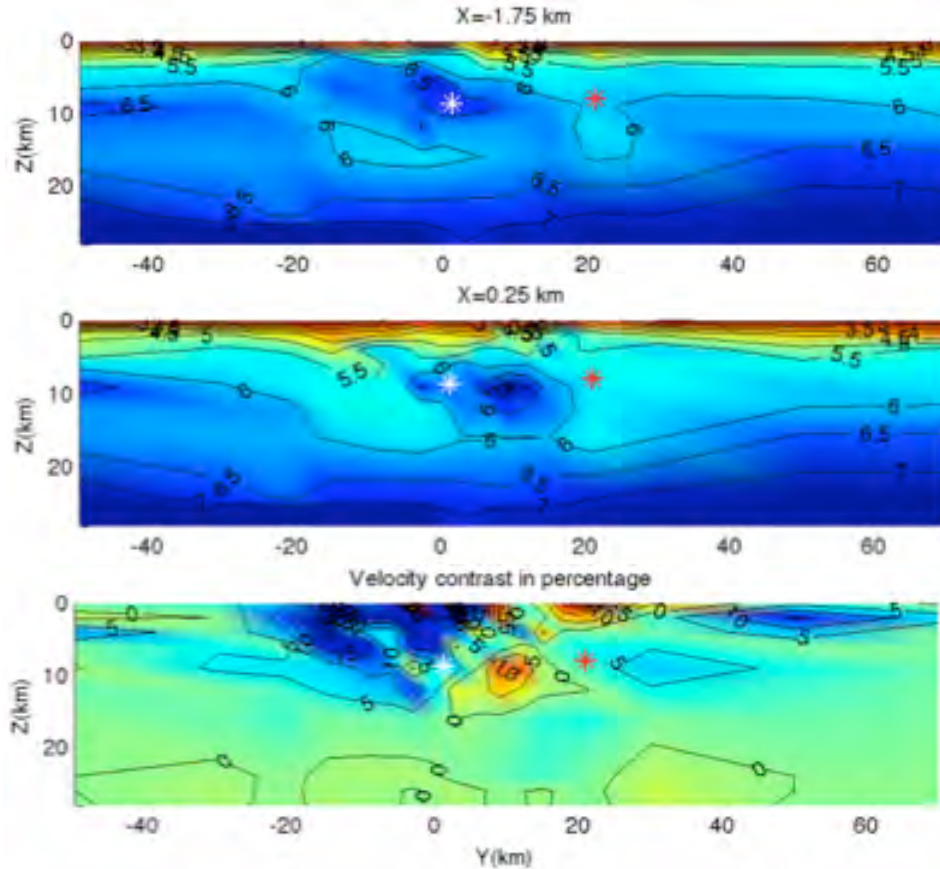


Figure 7. NW-SE cross-sections parallel to the SAF at the indicated X coordinate values (see inset in Figure 5) showing (top) the velocities just NE of the SAF, (middle) the velocities just SW of the SAF, and (bottom) the across-fault contrast. Note the correspondence between the locations of the 1966 and 2004 Parkfield hypocenters and the area of negative contrast (NE side fast) in between them corresponding to a high-velocity body on the NE side of the fault.

First, we compare seismicity along the fault-parallel section to the velocity contrast (Figure 8, top panel). We see that the creeping zone with abundant microseismicity is associated with the positive contrast areas, whereas the negative contrast area is nearly devoid of microseismicity. Next, we consider an along-fault section showing b-value (Schorlemmer et al., 2004) (Figure 8, middle panel). We find an excellent correspondence between low b-value areas southeast of SAFOD and the negative velocity contrast area, and similarly the match is clear between the moderate b-value area northwest of SAFOD and the positive velocity contrast area. Finally, we compare the Barnhart & Lohman (2010) slip contour of 30 cm for the 2004 Parkfield earthquake to the velocity contrast plot (Figure 8, bottom panel). Note that except for a difference in depth, there is a good match between the slip contour and the negative contrast area. It is also interesting to note that the slip contour is bounded both by the positive velocity contrast and large negative velocity contrast (i.e., > 10%), suggesting that active faults with comparable velocities (and strengths) on both sides can store elastic strain energy and release in large brittle failure events (Michael & Eberhart-Phillips 1991; Eberhart-Phillips & Michael, 1993).

In summary, we have succeeded in incorporating FZHW's and DWSA's in a formal tomographic inversion for velocity structure. Our results show that this approach produces a clear sharpening of the velocity contrast across the fault in the 3D tomographic model. Furthermore, comparison of the resulting velocity contrast to other geophysical observations shows that the velocity contrast variations are strongly related to the variations in microseismicity, b-value, and fault slip behavior.

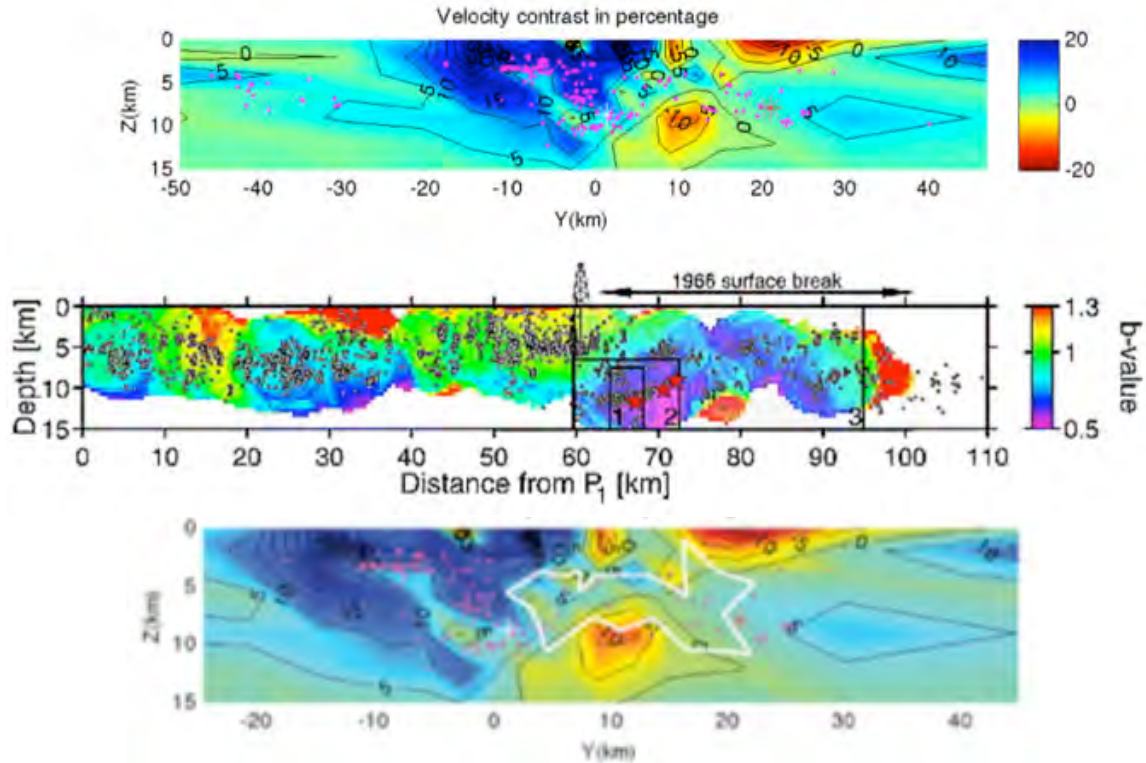


Figure 8. (Top) Seismicity along the fault-parallel section compared to the velocity contrast, showing that the creeping zone with abundant microseismicity is associated with the positive contrast areas (blue) whereas the negative contrast area (yellow-orange) is nearly devoid of microseismicity. (Middle) An along-fault section showing b-value (Schorlemmer et al., 2004) - note the excellent correspondence between low b-value areas (blue-purple) southeast of SAFOD and the negative velocity contrast area in the top panel, and similarly the match between the moderate b-value area (green) northwest of SAFOD and the positive velocity contrast area in the top panel. (Bottom) Comparison of Barnhart and Lohman (2010) slip contour of 30 cm (white line) for the 2004 Parkfield earthquake to the velocity contrast plot - note that except for a difference in depth, there is a good match between the slip contour and the negative contrast area.

References

- Barnhart, W. D., and R. B. Lohman (2010), Automated fault model discretization for inversions for coseismic slip distributions, *J. Geophys. Res.*, *115*, B10419, doi:10.1029/2010JB007545.
- Ben-Zion, Y. (1989), The response of two joined quarter spaces to SH line sources located at the material discontinuity interface, *Geophys. J. Int.*, *98*, 213–222.
- Ben-Zion, Y. (1990), The response of two half spaces to point dislocations at the material interface, *Geophys. J. Int.*, *101*, 507–528.
- Ben-Zion, Y., & K. Aki (1990), Seismic radiation from an SH line source in a laterally heterogeneous planar fault zone, *Bull. Seism. Soc. Am.*, *80*, 971–994.
- Ben-Zion, Y., S. Katz, & P. Leary (1992), Joint inversion of fault zone head waves and direct P arrivals for crustal structure near major faults, *J. Geophys. Res.*, *97*, 1943–1951.
- Ben-Zion, Y. & P. Malin (1991), San Andreas fault zone head waves near Parkfield, California, *Science*, *251*, 1592–1594.
- Bulut, F., Y. Ben-Zion and M. Bonhoff (2012), Evidence for a bimaterial interface along the Mudurnu segment of the North Anatolian Fault Zone from polarization analysis of P waves, *Earth Planet. Sci. Lett.*, in press, doi:10.1016/j.epsl.2012.02.001.

- Eberhart-Phillips, D. & A. J. Michael (1993), Three-dimensional velocity structure, seismicity, and fault structure in the Parkfield region, central California, *J. Geophys. Res.*, 98, 15,737–15,758.
- Haslinger, F., & E. Kissling (2001), Investigating effects of 3-D ray tracing methods in local earthquake tomography, *Phys. Earth Planet. Int.*, 123, 103-114.
- Hickman, S., M. Zoback, and W. Ellsworth (2004), Introduction to special section: Preparing for the San Andreas Fault Observatory at Depth, *Geophys. Res. Lett.*, 31, L12S01, doi:10.1029/2004GL020688.
- Hickman, S., M. Zoback, W. Ellsworth, N. Boness, P. Malin, S. Roecker, and C. Thurber (2007), Structure and properties of the San Andreas Fault in central California: recent results from the SAFOD experiment, *Scientific Drilling, Special Issue No. 1*, 29-32, doi:10.0/iodp.sd.s01.9.007.
- Hickman, S., M. Zoback, W. Ellsworth, J. Chester, F. Chester, J. Evans, D. Moore, D. Kirschner, A. Scleicher, B. van der Pluijm, and J. Solum (2008), Structure and composition of the San Andreas fault in central California: Recent results from SAFOD sample analyses: *EOS Transactions, American Geophysical Union*, 89, Fall Meeting Supplement, abs. T53F-01.
- Lengliné, O., & D. Marsan (2009), Inferring the coseismic and postseismic stress changes caused by the 2004 Mw = 6 Parkfield earthquake from variations of recurrence times of microearthquakes, *J. Geophys. Res.*, 114, B10303, doi:10.1029/2008JB006118
- Lewis, M. A, Y. Ben-Zion & J. McGuire (2007), Imaging the deep structure of the San Andreas Fault south of Hollister with joint analysis of fault-zone head and direct P arrivals, *Geophys. J. Int.*, 169, 1028–1042, doi: 10.1111/j.1365-246X.2006.03319.x.
- McGuire, J., & Y. Ben-Zion (2005), High-resolution imaging of the Bear Valley section of the San Andreas fault at seismogenic depths with fault-zone head waves and relocated seismicity, *Geophys. J. Int.*, 163, 152-164.
- McLaughlin, R. J., W. V. Sliter, D. H. Sorg, P. C. Russell, & A. M. Sarna-Wojcicki (1996), Large-scale right-slip displacement on the east San Francisco Bay region fault system, California: implications for location of late Miocene to Pliocene Pacific plate boundary, *Tectonics* 15 ,1-18.
- Michael, A. J., & D. M. Eberhart-Phillips (1991), Relationships between fault behavior, subsurface geology, and three-dimensional velocity models, *Science*, 253, 651-654.
- Schorlemmer, D., S. Wiemer, and M. Wyss (2004), Earthquake statistics at Parkfield: 1. Stationarity of b values, *J. Geophys. Res.*, 109, B12307, doi:10.1029/2004JB003234.
- Thurber, C., S. Roecker, H. Zhang, S. Baher, & W. Ellsworth (2004), Fine-scale structure of the San Andreas fault and location of the SAFOD target earthquakes, *Geophys. Res. Lett.*, 31, L12S02, doi: 10.1029/2003GL019398.
- Thurber, C., H. Zhang, F. Waldhauser, J. Hardebeck, A. Michael, & D. Eberhart-Phillips (2006), Three-dimensional compressional wavespeed model, earthquake relocations, and focal mechanisms for the Parkfield, California, region, *Bull. Seismol. Soc. Am.*, 96, S38-S49.
- Um, J., & C. Thurber (1987), A fast algorithm for two-point seismic ray tracing, *Bull. Seism. Soc. Am.*, 77, 972-986.
- Zhang, H. & C. Thurber (2003), Double-Difference Tomography: The Method and Its Application to the Hayward Fault, California, *Bull. Seismol. Soc. Am.*, 93(5), 1875-1889; DOI: 10.1785/0120020190.
- Zhang, H., C. Thurber, & P. Bedrosian (2009), Joint inversion for Vp, Vs, and Vp/Vs at SAFOD, Parkfield, California, *Geochem. Geophys. Geosyst.*, 10, Q11002, doi:10.1029/2009GC002709.
- Zhao, P., and Z. Peng (2008), Velocity contrast along the Calaveras fault from analysis of fault zone head waves generated by repeating earthquakes, *Geophys. Res. Lett.*, 35, L01303, doi:10.1029/2007GL031810.
- Zhao, P., Z. Peng, Z. Shi, M. Lewis, and Y. Ben-Zion (2010), Variations of the velocity contrast and rupture properties of M6 earthquakes along the Parkfield section of the San Andreas fault, *Geophys. J. Int.*, 180, 765-780, 10.1111/j.1365-246X.2009.04436.x.
- Zoback, M., S. Hickman, & W. Ellsworth (2011), Scientific drilling into the San Andreas fault zone - an overview of SAFOD's first five years, *Scientific Drilling*, 11, 14-28.

(4) Bibliography

Bennington, N., C. Thurber, H. Zhang, Z. Peng, and P. Zhao (2011), Incorporating fault zone head wave and direct wave secondary arrival times into seismic tomography: Application at Parkfield, California, Abstract T13G-02 presented at 2011 Fall Meeting, AGU, San Francisco, Calif., 5-9 Dec.